Manuscript Details

Manuscript number	ENGEO_2018_304
Title	Assessing preferential seepage and monitoring mortar injection through an earthen dam settled over a gypsiferous substrate using combined geophysical methods
Article type	Research Paper

Abstract

ABSTRACT For several decades the Sant Llorenç de Montgai reservoir has experienced different problems that could affect the safety of the engineering structure. For this reason, several corrective actions have been taken over the years. Here, we present a study involving complementary geophysical methods including electrical resistivity tomography, seismic refraction tomography and frequency-domain electromagnetic surveys. The analysis of the inverted electrical resistivity tomography cross-sections combined with the seismic refraction results and land subsidence monitoring data show the likely mechanism of abnormal seepage. The areas where mortar injections were applied as a corrective measure are also clearly delineated. In addition, the evolution of the state of the embankment has been established from two successive electrical resistivity tomography surveys in the last two decades. The results show areas where corrective mortar injections have been effective, while in other areas new abnormal seepage has been detected. The lithological heterogeneity of the bedrock, especially the dissolution of gypsum-rich rocks, induced subsidence effects and caused abnormal seepage in different areas along the embankment. Our results indicate how corrective solutions can be optimised to reduce the cost of corrective engineering interventions.

Keywords	Seepage monitoring; mortar injection; earthen dam; geophysical methods; electrical resistivity tomography; seismic refraction.
Taxonomy	Geological Surveys, Geoelectrics, Applied Geophysics

Corresponding Author	Mahjoub Himi
Corresponding Author's Institution	Universitat de Barcelona
Order of Authors	Mahjoub Himi, Ismael Casado, Alex Sendros, Raúl Lovera, Lluis Rivero, Albert Casas

Suggested reviewers	Giorgio Cassiani, Oliver Kuras, Manuel João Senos Matias

Submission Files Included in this PDF

File Name [File Type]

cover letter Himi.pdf [Cover Letter]

highlights Himi- 2018.pdf [Highlights]

ABSTRACT.pdf [Abstract]

Assessing preferential seepage Himi et al EG 2018.pdf [Manuscript File]

Fig 1a-b.tif [Figure]

Fig 1c.tif [Figure]

Fig 2.tif [Figure]

Fig 3.tif [Figure]

Fig 4.tif [Figure]

Fig 5.tif [Figure]

Fig 6.tif [Figure]

Fig 7.tif [Figure]

Fig 8a.tif [Figure]

Fig 8b.tif [Figure]

Fig 9.tif [Figure]

Fig 10.tif [Figure]

To view all the submission files, including those not included in the PDF, click on the manuscript title on your EVISE Homepage, then click 'Download zip file'.

Research Data Related to this Submission

There are no linked research data sets for this submission. The following reason is given:
No data was used for the research described in the article

UNIVERSITAT DE BARCELONA

Himi Benomar, Mahjoub

Department of Mineralogy, Petrology and Applied Geology,
Marti i Franques, s/n 08007 Barcelona
Tel. +34 934 035 922 Fax +34 933 188 163 himi@ub.edu

Dear Editor-in-Chief

I am pleased to submit an original research article entitled “Assessing preferential seepage and monitoring mortar injection through an earthen dam settled over a gypsiferous substrate using combined geophysical methods.” by Himi, M.; Casado, I.; Sendros, A.; Lovera, R.; Rivero, L.; Casas. A. for consideration for publication in Engineering Geology Journal.

In this manuscript, we illustrates that the combination of different geophysical methods provides useful information for characterizing preferential seepage flow paths, so corrective interventions can be optimized, and therefore reduce the cost of remedial engineering works. The relationship between the physical parameters of geological materials has been successfully applied proving cost-effective information.

We believe that this manuscript is appropriate for publication by Engineering Geology Journal because the objectives and results of the study match with the targets of the journal.

This manuscript has not been published and is not under consideration for publication elsewhere. We have no conflicts of interest to disclose.

Thank you for your consideration

Sincerely,

Dr. Himi Mahjoub

Assessing preferential seepage and monitoring injection mortar through an earthen dam settled over a gypsiferous substrate using combined geophysical methods

Highlights

- The assessment of hazards related to earthen embankments settled over gypsiferous sediments susceptible to dissolution and consequently the formation of subsidence areas could play a negative role and lead to essential seepage.
- The embankment materials where fine particles are being washed out by seepage thus increasing the hydraulic permeability
- The changes in electrical resistivity and seismic velocity are partly related to the cement mortar injections and partly to the abnormal seepage.
- The results from the use of complementary geophysical methods allow optimal corrective interventions, thus reducing the cost of remediation.

ABSTRACT

For several decades the Sant Llorenç de Montgai reservoir has experienced different problems that could affect the safety of the engineering structure. For this reason, several corrective actions have been taken over the years. Here, we present a study involving complementary geophysical methods including electrical resistivity tomography, seismic refraction tomography and frequency-domain electromagnetic surveys.

The analysis of the inverted electrical resistivity tomography cross-sections combined with the seismic refraction results and land subsidence monitoring data show the likely mechanism of abnormal seepage. The areas where mortar injections were applied as a corrective measure are also clearly delineated.

In addition, the evolution of the state of the embankment has been established from two successive electrical resistivity tomography surveys in the last two decades. The results show areas where corrective mortar injections have been effective, while in other areas new abnormal seepage has been detected.

The lithological heterogeneity of the bedrock, especially the dissolution of gypsum-rich rocks, induced subsidence effects and caused abnormal seepage in different areas along the embankment. Our results indicate how corrective solutions can be optimised to reduce the cost of corrective engineering interventions.

Assessing preferential seepage and monitoring mortar injection through an earthen dam settled over a gypsiferous substrate using combined geophysical methods

ABSTRACT

For several decades the Sant Llorenç de Montgai reservoir has experienced different problems that could affect the safety of the engineering structure. For this reason, several corrective actions have been taken over the years. Here, we present a study involving complementary geophysical methods including electrical resistivity tomography, seismic refraction tomography and frequency-domain electromagnetic surveys.

The analysis of the inverted electrical resistivity tomography cross-sections combined with the seismic refraction results and land subsidence monitoring data show the likely mechanism of abnormal seepage. The areas where mortar injections were applied as a corrective measure are also clearly delineated.

In addition, the evolution of the state of the embankment has been established from two successive electrical resistivity tomography surveys in the last two decades. The results show areas where corrective mortar injections have been effective, while in other areas new abnormal seepage has been detected.

The lithological heterogeneity of the bedrock, especially the dissolution of gypsum-rich rocks, induced subsidence effects and caused abnormal seepage in different areas along the embankment. Our results indicate how corrective solutions can be optimised to reduce the cost of corrective engineering interventions.

1. INTRODUCTION

Earth embankments occasionally fail, in spite of safety measures and precautions taken to ensure their stability. There are three major causes of instability: 1) seepage and internal erosion within the embankment; 2) seepage and erosion of the foundation; and 3) overtopping (ICOLD, 1995). With adequate surveillance, the first two causes can be detected and remedied before failure occurs. Seepage through earth embankments is a major safety concern and can have extreme socio-economic consequences. These two processes constitute the second cause of catastrophic failure of earthen dams: some 46% of all documented failures (Foster et al., 2000). Internal erosion occurs when water flows through pores, cracks and other continuous voids within embankments. As the permeability increases due to the erosion of fine elements, the hydraulics of seepage zones also change over time. This can lead to the formation of piping and the development of subsurface voids (Ikard et al., 2015). These voids can be caused by many different factors, including inadequate compaction during construction, different settlement processes, desiccation, earthquakes, burrowing animals and the decay of woody plant roots. In these circumstances, grouting the dam foundation is an effective technique for improving the subsurface and maintaining the integrity of dams and their levees. Grouting is a process by which open geological defects are sealed by injecting a cement fluid to reduce seepage and/or strengthen the foundation. The grouting material may be based on a suspension of cementitious solids in water, different colloidal or chemical solutions, or a combination of both materials (Attewell and Farmer, 2012; Lee, et al., 2005; Uromeihy and Barzegari, 2007).

The early detection of weak zones is essential to prevent possible levee collapse and to establish the most appropriate solutions. If the leak proofing of a dam is not sufficient, remediation can

be carried out by traditional injection. The application of individual geophysical methods – electrical, electromagnetic or seismic – is usually considered suitable for studying and characterising dam seepage and subsidence (Benson et al., 2003; Cardarelli et al., 2014; Haile and Atsbaha, 2014; Gunn et al., 2015; Loperte et al., 2016). Nevertheless, a combination of different techniques has achieved more effective results (Pislaru-Danescu et al., 2013; Maslakowski et al., 2014). Abnormal seepage entails a significant variation in the moisture/water content inside the structure, which is associated with an increase in electrical conductivity (Ikard et al., 2014). Two-D high-resolution images of the electrical conductivity in the area studied can be produced using electrical resistivity tomography (ERT) and thus help diagnose leakage problems. Together with seismic refraction tomography (SRT), ERT is one of the leading techniques for assessing civil engineering structures and examining seepage (Johansson and Dahlin, 1996; Benson et al., 1997; Kim et al., 2007; Osazuwa, 2009).

Our research was conducted on a problematic old earthen dam in Sant Llorenç de Montgai (Lerida, Spain). The bedrock consists mostly by Triassic clays and Eocene marls with some traces of gypsum, both of which are susceptible to dissolution. Consequently, there is seepage beneath the dam, as evidenced by the presence of subsidence zones that have formed in the bottom of the reservoir. This has resulted in efforts to reduce the seepage beneath the dam. Remediation measures have included the construction of grout curtains. Nevertheless, seepage continues to be a concern. The objective of our study was to monitor the penetration of mortar into the ground by defining its area and geometry, and identifying the key seepage areas along the embankment. The geophysical results were also correlated with land subsidence monitoring along the embankment.

2. MATERIALS AND METHODS

2.1. STUDY AREA, MATERIALS AND STATE OF THE LEVEE

The Sant Llorenç de Montgai dam (NE Spain) is located about 150 km west of the city of Barcelona. The dam was built in 1935 to regulate the downstream flow of the Segre River for the purposes of irrigation and power generation. The structure of the dam combines a 164 m long concrete barrage and an 860 m long earthen embankment. The whole structure rests on Quaternary alluvial sediments composed of gravel, sand and silt which in turn cover a substrate that is composed primarily of Mesozoic sediments (Triassic Keuper gypsum and red clays, and Jurassic/Cretaceous dolomites and limestones) and Eocene marls and limestones (Fig. 1a). According to the geological map, the bedrock under the water reservoir consists mostly of marls with some thin gypsum veins, both of which are exposed to dissolution by unsaturated fresh water (Fig. 1c).

The embankment consists of a 10 m wall of alluvial material (mainly gravel and sand), covered by 3 m of soil. Before the embankment was erected, a trench was excavated in the Quaternary sediments down to the impervious layer of clays and marls. The space created was filled with bentonite clays to waterproof one side of the wall. In addition, a 36 m long concrete structure attached to the impermeable layer was built stretching out from the dam (Fig. 2.b).

Since its construction, the embankment has often been affected by seepage that has required maintenance in order to reduce water loss and safeguard the stability of the structure. On the basis of technical reports, the main maintenance surveys are summarised in what follows.

As soon as the reservoir was filled in 1930, some leaks appeared in the embankment and the agricultural field behind it was flooded. In order to improve water drainage downstream from

the river, a concrete collector was then build and a water flow meter installed. The embankment also presented some settlement and small landslides on both slopes, which were resolved by the injection of clay and cement mortar. In July 1939, 1800 tonnes of clay and 340 tonnes of cement mortar had been injected, resulting in a reduction of 25% of the total leakage, as measured at the end of the collector drain.

The corrective actions continued to gradually reduce the flow from leaks; in March 1950, leakage in the area of the drainage ditch had been reduced by 80%. The reservoir was therefore not totally waterproof, but the amount of water filtering out was admissible. The dam and its surroundings were subject to regular inspections. In addition, the reservoir was periodically emptied in order to inspect the rafts of the floating automatic gates, examine the reservoir bed and fill any sinkholes detected (Figures 2a and 2c).

During the 1980s, remediation work stopped, which resulted in some settlement in the dyke due to a loss of fine materials caused by leakage, and some significant sinkholes were detected in 1990. For this reason, four surveys (1990-1993) were conducted leading to a new plan to inject and waterproof the screen along the embankment. The aim was to repair settling surfaces, replace the eroded material and reinforce the impervious barrier. About 1200 tonnes of mortar and 672 m^3 of sand were injected between hectometres 0.30-1.60, 2.00-4.30 and 6.00-8.60. In addition, a set of benchmarks for precise levelling was installed along the dyke. At the same time, to accompany the injections, a waterproof PVC screen was installed under the stone slope, in contact with the water reservoir between levels 284.50 and 287.00 m a.s.l. The result of the injections and waterproofing actions was positive; nevertheless, seepage continues to be a concern.

2.2. GEOPHYSICAL METHODS

Three complementary geophysical methods were applied to study the internal structure and subsurface beneath the embankment: electrical resistivity tomography (ERT), seismic refraction tomography (SRT) and frequency-domain electromagnetics (FDEM). All the profiles were referenced to the dam hectometre points, with the starting point located close to the concrete dam structure, from south to north (Fig. 2a).

DC resistivity is an effective geophysical tool in dam seepage studies because it is sensitive to changes in lithology, water saturation and water chemistry (Binley and Kemna, 2005). ERT has been widely implemented in the earth sciences in recent years due to the quality of the data obtained and the fact that it can provide continuous 2D and 3D underground images (Panthulu et al., 2001; Cho and Yean, 2007; Sjödahl et al., 2010). The ERT surveys were performed along the eastern part of the dam using a SYSCAL Pro 48 resistivity meter. A Schlumberger reciprocal array was selected, because it is less sensitive to noise than the dipole–dipole array (Dahlin and Zhoo, 2004). In order to study the evolution of electrical resistivity values, we performed the survey in two campaigns: 2003 and 2012. In the two survey periods, the acquisition profiles were performed by concatenating the first 24 electrodes of all profiles until the entire levee line was surveyed. In this way, we can represent separate profiles or concatenated profiles. The concatenate option from RES2DINV (Loke and Barker, 1996) inversion software has been set to compile different segment together in one profile, but without giving up representing the results of each profiles separately. The spacing between adjacent electrodes was 2 m for the two campaigns. In 2012, we also acquired profiles with a distance of 5 m between adjacent electrodes using the same technique, these profiles made it possible to obtain lines that were 235 m long and to reach 40 m depth .

All of the apparent resistivity pseudosections were inverted using RES2DINV software (Geotomo, 2007), which transform the apparent resistivity of samples to calculated resistivity values through an inversion process, based on a smoothness-constrained least-squares method (De Groot-Hedlin and Constable, 1990). Moreover, in order to eliminate all possible artefacts created in the "shadow areas", only the upper part of the inverted sections was used in the concatenated profiles. All the profiles were referenced to the hectometre points of the dam, with the first profile starting at distance 0 (in the south) and the last profile finishing at distance 770 m (in the north) (Fig. 2. a).

SRT profiles were acquired along the right border of the earthen embankment, in accordance with the ERT profile lines. The purpose of the survey was to obtain a detailed seismic velocity distribution along the earthen embankment and from it infer the degree of inhomogeneity of the core clay and its distribution. The data from 10 profiles were collected using a 24-channel DAQ Link III seismograph with 4.5 Hz vertical geophones. The distance between the geophones was 3 m, and they were embedded in the ground for optimum physical contact. Each profile was a total of 75 m in length. Since for safety reasons it was not possible to use an energy source, we used sledgehammer impacts on a steel plate as the source of seismic waves for all the profiles. Nine shots were used for each line. The first and last shots were made at a distance of -3 and +3 m, respectively, from the first and the last geophones, while the other seven shots were evenly distributed along the line. The hammer shots were added four times in order to check the effects of noise and enhance the signal. Noise was monitored in real time alongside data collection to make sure that the noise level was significantly reduced each time a dataset was collected. Of the 10 profiles recorded, only seven were processed, since the first three where close to the dam turbines, which caused very strong vibrations and made it difficult to establish the first arrival times. Figure 3 shows two seismic refraction records: one recorded at the beginning of the dam (at the distance 0 m) and close to the hydroelectric plant (Fig.3a); the second at 200 m from the beginning of the dam (Fig.3b).

Multiple vertical strikes per source position were used to create single high-quality records, which were then stored as SG2 files. The processing, velocity calculation and modelling of the seismic section were all performed with the Rayfract® software package. Once the first arrival time breaks for all refractors had been assigned, the travel time data were processed with the smooth inversion method (Rohdewald, 2010), using Rayfract® software version 3.18. Smooth inversion first automatically determines an initial 1D model directly from the picked travel times, using the DeltatV method (Gebrande and Miller, 1985; Gebrande, 1986; Gibson et al., 1979). This initial 1D model is then iteratively refined using 2D wavepath eikonal traveltime (WET) tomographic inversion.

Frequency-domain EM were measured using a Geonics EM31 instrument. The system consists of transmitting and receiving coils spaced 3.66 m apart and operates at a frequency of 9.8 kHz. When operated at a low induction number, i.e. where the electromagnetic skin depth greatly exceeds the transmitter/receiver coil space, the instrument provides the apparent, or depth-averaged, conductivity at each measurement position (McNeill, 1980; McNeill, 1990; Fitterman and Labson, 2005; and Pérez-Flores et al., 2011). In our case, two ground conductivity measurements were performed on each station. The coils can be positioned either in a vertical (VD) or horizontal (HD) dipolar configuration. The horizontal coil configuration was used to estimate the conductivity of the first 3 meters. In this mode the sensitivity of the response to the subsurface conductivity is highest at the surface and decreases with depth. The vertical configuration estimates the first 6 meters. In this case, the sensitivity increases from zero at the

surface to a maximum at a depth of 1.3 m, and then decreases with depth. In all the measurements, the spacing between stations was 1 m.

3. RESULTS

For all the ERT profiles, the results of the inversion process showed a root mean square error lower than 7% after five iterations and an apparent resistivity contrast of less than 300 Ωm. According to the variation and distribution of the electrical resistivity values, all resistivity sections respond to a three layers model (Fig. 4):

- An upper low-resistivity layer (ULRL) with electrical resistivity values less than 100 Ωm and a thickness of about 5 m. This layer shows some exceptions in many areas where the resistivity values are higher than the expected values (ERT-1: at 32 and 64 m, ERT-7: at 330 m; ERT- 9: at 380 m; ERT- 13: at 590 and 640 m; …).
- An intermediate high resistivity layer (IHRL), with more than 400 Ωm. The thickness of this layer is not constant and generally reaches a depth of up to 15 m. As the upper level, the intermediate layer also shows some exceptions vis à vis the distribution of resistivity values, since areas with values much lower than the expected values were registered (ERT-9: at 365, 395 and 425 m; ERT-11: at 490 m; ERT-13: at 595 m; …).
- A deeper low resistivity layer (DLRL) registered in all sections between 13 and 15 m depth and with a resistivity values less than 70 Ωm.

According to the dam construction reports, the upper and intermediate layers respectively correspond to electrical response of clay (low resistivity) and sand, gravel (high resistivity), whereas the bottom conductive layer is related to different bedrock present under the dam structure, and mostly consist of clay and marls, with some gypsum veins exposed to dissolution.

The high values registered in the upper and intermediate layers which are not consistent with the normal values of geological materials have been interpreted as a result of the mortar injections carried out to reduce seepage through the embankment. While the abnormal low resistivity values lead us to assume that the materials are saturated due to infiltration from the reservoir.

A comparison between the two geophysical surveys carried out in 2003 and 2012 shows similar inverted resistivity cross-sections (Fig. 5). However, there are some specific differences in the distribution of the resistivity values. These differences are observed in individual profiles and even more in the concatenated profiles. In effect, on one hand, we observe a decrease in the abnormal seepage areas registered in the 2003 profiles at the distances of 75, 370 and 400 m from the beginning of the profile, which have subsequently been filled with mortar (resistivity values higher than 600 Ωm); and on the other hand, new areas with low resistivity values (less than 50 Ωm), observed in the 2012 profiles at the distances of 50, 450 and 550 m and which would indicate a deterioration of the embankment as a result of new abnormal seepages.

The results for the long ERT profiles (235 m length with a distance between electrodes of 5 m) show a similar distribution of the electrical resistivity values than the short profiles (2 m between electrodes). The fact that the spacing between electrodes is greater, makes the depth investigation greater, since we reach 40 m (Fig. 6). However, we observed a diminution in the resolution of the profiles both vertically (we cannot distinguish exactly the position of the contact between the three levels) and horizontally (it is not possible to detect small areas of mortar injection or abnormal seepage).

The concatenated ERT profile (Fig. 6) show a lateral change of electrical resistivity, with a clear decrease of values at the distance 400 m and which we interpret as a seepage area. We observe also a slight change of resistivity values in the deep part of the profile, which indicates a change in the bedrock materials.

The EM-31 profile shows the HD and VD conductivity patterns along the dam embankment. Conductivity values were represented in a binary plot which shows that EM signals along the embankment may be related to the presence of material with high or low electrical conductivity inside the levee. The apparent conductivity profiles of the two coil configurations show a similar trend, but with different values of conductivity. VD reflects values higher than HD (Fig. 7a). This is due to HD being more sensitive to lateral variations, while VD is more sensitive to variations in depth (McNeill, 1980). The figure 7 shows areas with clearly high electrical conductivity values at distances of 80, 390 and 740 m. We have interpreted these anomalies of high electrical conductivities (blue colour on the Fig. 7b) as a consequence of the seepage areas detected previously with the ERT.

The seismic record data was processed and inverted. The 1D initial model still shows a good initial travel time fit between measured and picked times (Figure 8.a). In all the profiles, the data that were observed and calculated have a difference in RMS error of less than 5%. Seismic travel time tomography requires optimisation of both the distribution of seismic velocities and the paths along which the wave has travelled, or ray paths. Figure 8.b displays the distribution of ray paths corresponding to the optimum solution. The obvious use of this map is to establish the relative sampling of the subsurface. Results in areas with low ray coverage would have lower confidence than areas of high ray coverage (Hickeyet al., 2010). Rayfract^{TM} uses the ray coverage map to establish spatial bounds on the velocity tomogram. For this survey, the ray coverage is highest in the middle of the survey and lower near the surface and edges, which is typical for a material with a fairly uniform vertical velocity gradient. The inverted velocities from the refraction analysis showed multiple velocity intervals, from the surface to the base. This shows that there are several strata within the overburden, with variable thicknesses and velocities. In general, the velocity increases with depth, from about 300 m/s near the surface to more than 2000 m/s (Fig. 9). The corresponding velocities indicate a three-layered structure. The upper layer with low velocity values of under 1000 m/s was recorded in all profiles. Although the average thickness of this layer is about 4 m (profiles 1 and 3), some stations recorded thicknesses greater than 5 m (the stations at the distances 290, 370 and 400 m), while other stations registered thicknesses of less than 2 m (at distances 230, 275, 330 and 455). The intermediate seismic layer has values between 1000 and 1800 m/s, and reaches an average depth of between 12 and 14 m in all profiles except P4 and P6, where it goes deeper. Below these two seismic layers lie a layer with a significantly higher velocity (above 2000 m/s). This layer appears at a depth of less than 10 m in profile 7.

The vertical changes in velocity with depth are related to lithological changes; therefore, the shallow low-velocity layer corresponds to clay, the intermediate layer to sand and gravel and finally, the deeper high-velocity layer corresponds to marl. The lateral changes in seismic velocity are interpreted as changes in density of the same lithology when the velocity is lower, and as a consequence of mortar injections when the velocity is higher.

4. DISCUSSION

Based on the information from the dam construction reports, the layer between the surface and -15 m in depth are related to the upper part of the levee, which is mainly formed by gravel and sand. This depth is related primarily to the first two upper layers in the ERT and SRT profiles. As mentioned, inverted resistivity values vary along the levee, and are particularly changeable in

the intermediate layer (Fig. 4). If it is assumed that the variations in resistivity values are usually caused by lithological differences or by changes in the properties of the medium itself (Chinh, 2000; Sudha et al., 2009; Casado et al., 2015), and that the levee materials would respond equally to the different geophysical methods along the levee, then the changes in the upper layers will be related to alterations in the physical properties of the levee materials. In this particular study, modifications in the degree of humidity of the levee materials (sand and gravel) and the presence or absence of mortar injections produced changes in the resistivity values.

In terms of the electrical methods, abnormal seepage entails a significant variation in the moisture/water content inside the structure, which is associated with an increase in electrical conductivity (Loperte, 2015). Nevertheless, the presence of mortar injections leads to natural pore spaces becoming clogged with the mortar, thus reducing saturation and increasing electrical resistivity (Farooq et al., 2013). Seokhoon (2012) proposes that the variation in resistivity due to damage to core materials after treating a damaged section by grouting produces an increment in resistivity values. Accordingly, the relatively high electrical resistivity values (Fig. 4) in the intermediate layer (>300 Ωm) may correspond to dry sand and gravel that did not undergo much alteration from the mortar injections and were not affected by abnormal seepage . Where gravel and sand have been affected by abnormal seepage, resistivity values in the intermediate level drastically drop to below 100 Ωm and could be defined and characterised. However, in those areas where resistive response presents the highest values (>800 Ωm), these are related to the locations where mortar injections persist over time without alteration. To confirm these observations, we have checked the records of the injections takes out in the embankment between 1991 and 2009 as corrective measures of the infiltrations during the remediation works (Fig. 10). The high electrical resistivity values registered between the distances 0 and 320 m coincide with the position of the last mortar injections (2009). On the other hand, the low electrical resistivity anomaly registered in 2012 in the intermediate level at the distances 50, 440, 550 m could indicate a deterioration of the embankment and possible new abnormal seepage under this area.

The long ERT profiles (5 m between electrodes) provided interesting information about the state of the bedrock under the dam due to the greater depth of investigation and the possibility to correlate them with the available geological information. As can be seen in the geological section of figure 1, the center of the dam coincides with the passage of a thrust fault, which separates the Tx unity (Triassic Clays and Gypsum) and the Om unity (Gypsiferous Marls). This geological discontinuity coincides with the electrical discontinuity registered in the ERT profile at 400 m from de beginning of the dam (Figure 6). The lithological characteristics of these formations (gypsum and shale) and previous records concerning the dissolution of this unit on the reservoir bed (Canals et al., 1994), may indicate the presence of deep filtration routes under the embankment. The presence of several sinkholes found when the dam has been emptied for maintenance work confirms this hypothesis. In effect, a significant instability was induced by the dissolution of the basement material. The Fig. 10 shows the areas where the subsidence was most pronounced along the embankment. This area was also located between the beginning and 400 m away.

With regard to the seismic behaviour of the embankment materials, the main differences in wave velocities are generated by the grade of material consolidation beneath the surface. Unconsolidated materials such as clay, gravel and sand record the lowest range of wave velocities, while consolidated materials such as rock formations cause the highest velocities (Han et al., 1986, Goldberg and Gurevich, 1998). In the shallow environment, a common type of

lateral inhomogeneity is the narrow low-velocity zone in unweathered rock. According to Palmer (1991), such zones have been attributed to shearing and the weathering of dikes. They are usually associated with an increase in the thickness of the weathered layer. The definition of these features is important in geotechnical studies because they represent areas of weak rock and usually high porosity and permeability (Palmer, 1991). Therefore, the increase in velocity with depth can be explained by the levee material disposition. Low velocities could be associated with the unconsolidated nature of the clay construction materials. These weaker formations are permeable zones within the subsurface of the embankment through which water seepage takes place. These results agree with the results obtained by Osazuwa and Chinedu (2008) who show that a low-velocity zone can be attributed to unconsolidated and loose material within the overburden, where most highly permeable seepage channels occur. Moderate-velocity zones close to the surface might represent the gravel and sand that form the levee; while the deepest high-velocity layer might correspond to the bedrock. In fact, the velocity of the deepest layer (over 1975 m/s) is consistent with the results of Pavlovic and Velickovic (1998), who demonstrated that the velocity of clay-based materials varies from 1200 to 2500 m/s. However, some seismic sections (profiles 2, 4, 6 and 7; Fig. 9) showed relatively high-velocity zones (around 1600 m/s) near the surface. These areas might correlate with the mortar injections which reduce the porosity of unconsolidated materials and therefore increase their compaction and P wave velocities (Busato et al., 2016). In areas where the velocities were lower than expected, even at significant depths (8 m in the case of profiles 5 and 6), these were attributed to preferential water circulation areas with internal erosion, which therefore created seepage areas. This result is consistent with the results of Akin (2016), who carried out some experiments on material used for jet grouting and demonstrated the presence of very strong negative linear relationships between Vp and porosity.

The comparison between the results obtained by the different geophysical methods shows that the areas where the electrical resistivity values (ERT) are lower than the expected values coincide with the areas of high electrical conductivity (EM31) and accord with areas of low seismic velocities. These zones are located at the distances 80, 400 m and coincide with seepage areas. Whereas , the areas with high electrical resistivity (ERT) coincides with low electrical conductivities (EM31) and with high seismic velocities. These anomalies are a consequence of areas of mortar injections (225,300, 640 m)

5. CONCLUSIONS

On the basis of the geophysical analysis carried out on the Sant Llorenç de Montgai dam embankment, we conclude that combined ERT, SRT and FDEM represent a valid and fast method to study seepage areas and to define the expansion of mortar injected along the embankment.

By virtue of ERT, several areas have been identified in the embankment as anomalous resistivity zones with respect to the expected resistivity values. The low values (less than 50 Ωm) have been related to seepage zones caused by the dissolution of bedrock gypsum materials, and or as a result of the internal erosion which appears within the embankment materials where fine particles are washed-out and subsequently saturated. In contrast, areas of high resistivity are associated with corrective mortar injections.

Seepage through the dam can be qualitatively evaluated by comparing different areas of the dam at different times. The electrical resistivity results obtained in 2012 showed significant changes with respect to previous surveys. The changes are due partly to the cement mortar

injections, which are reflected in increased resistivity values, and partly to the new filtration zones that appear as areas of low resistivity.

The continuous acquisition of data using ERT over the course of many years can be considered a useful technique for assessing and planning new remediation interventions in areas with possible infiltration problems.

The seismic data reflect increasing velocity with depth as a consequence of increased material compaction. High seismic velocity anomalies were related to mortar injection areas, while low seismic velocities were related to porous areas.

The seismic data indicate a change of materials, both laterally and with depth. The increment of P waves velocity with depth is attributed to the passage from clays to sand and gravels and finally to the gypsum bedrock, while the lateral variation is related to mortar injection when the P waves velocity is high and to seepage areas when the velocity is low than the expected values.

We observed a limitation of the FDEM method (EM31) compared to ERT or SRT, especially the resolution of the method.

Finally, we feel strongly that the methodology has yielded information that can greatly help to characterise preferential seepage flow paths through the Sant Llorenç de Montgai dam, so corrective interventions can be optimised, thus reducing the cost of remedial engineering works.

Finally, we feel strongly that the methodology has yielded information that can greatly help to characterise preferential seepage flow paths, so corrective interventions can be optimised, and therefore reduce the cost of remedial engineering works.

ACKNOWLEDGEMENTS

This study was funded and supported by ENEL (Ente Nazionale per l'Energia Elettrica) (formerly ENDESA - Empresa Nacional de Energía Eléctrica), the current owner of the Sant Llorenç de Montgai dam. The authors thank Francisco Conesa and Carlos Quintillá from ENEL.

REFERENCES

Akin M.A., 2016. Experimental studies on the physico-mechanical properties of jet-grout columns in sandy and silty soils. Journal of African Earth Sciences, 116. 190-197.

Attewell P. B., & Farmer I. W. 2012. Principles of engineering geology. Springer Science & Business Media.

Benson A.K., Payne K.L., Stubben M.A., 1997. Mapping groundwater contamination using DC resistivity and VLF geophysical methods-A case study. Geophysics 62, 80–86

Benson R.C., Yuhr L., Kaufmann R., 2003. Some considerations for selection and successful application of geophysical methods. Third International Conference on Applied Geophysics, Geophysics 2003, December 8-12, Orlando, Florida.

Binley A., Kemna A., 2005. DC resistivity and induced polarization methods, in: Hydrogeophysics, Ruben Y., Hubbard S. eds., Springer, Dordrecht, The Netherlands, pp. 129-156.

Busato L., Boaga J., Peruzzo L., Himi M., Cola M., Bersan S., Cassiani G., 2016. Combined geophysical surveys for the characterization of a reconstructed river embankment. Engineering Geology. 211, 74-84.

401 Canals M., Casas A., Carmona J.M., Casamor J.L., Font X., Calafat A.M., 1994. Metodos geofísicos
402 aplicados al estudio y localización de fugas en embalses. Tomo 2. Edita. Canals & Casas.
403 Cardarelli E., Cercato M., De Donno G., 2014. Characterization of an earth-filled dam through
404 the combined use of electrical resistivity tomography, P- and SH-wave seismic
405 tomography and surface wave data. J. Appl. Geophys. 106, 87–95.
406 Casado I., Himi M., Lovera R., Fernández J., Casas A., 2015. Use of electrical tomography methods
407 to determinate the extension and main migration routes of uncontrolled landfill
408 leachates in fractured areas. Science of the Total Environment, 506, 546-553.
409 Chinh P., 2000. Electrical properties of sedimentary rocks having interconnected water-
410 saturated pore spaces. Geophysics; 65(4): 1093–1097.
411 Cho I.-K., Yeom J.-Y., 2007. Crossline resistivity tomography for the delineation of anomalous
412 seepage pathways in an embankment dam. Geophysics, 72(2), G31–G38.
413 Hickey C.J., Ekimov A., Hanson G.J., and Sabatier J.M., 2009. Time-Lapse seismic measurements
414 on a small earthen embankment during an internal erosion experiment. Symposium on
415 the Application of Geophysics to Engineering and Environmental Problems 2009: pp.
416 144-156.
417 Dahlin T., Zhoo B., 2004. A numerical comparison of 2D resistivity imaging with 10 electrode
418 arrays. Geophysical Prospecting. 52, 379-398.
419 De Groot-Hedlin C., Constable S., 1990. Occam's inversion to generate smooth, two-dimensional
420 models from magnetotelluric data. Geophysics 55, 1613-1624.
421 Farooq M., Park S., Song Y.S., Kim J.H., Sabir M.A., Umar M., 2013. Application of electrical
422 resistivity method to evaluate the extent of mortar infiltration in subsurface cavities.
423 Arab J Sci. Eng. 38, 111-120.
424 Fitterman D.V., Labson V.F., 2005. Electromagnetic induction methods for environmental
425 problems D.K. Butler ed., Near-surface Geophysics, Society of Exploration Geophysicists,
426 Oklahoma, USA. pp. 301–356
427 Foster M., Fell R., Spannagle M., 2000. The statistics of embankment dam failures and accidents.
428 Canadian Geotechnical Journal 37, no. 5: 1000–1024.
429 Gebrande H., Miller H., 1985, Refraktionsseismik, in: Angewandte Geowissenschaften II.
430 Ferdinand Enke Verlag, Stuttgart, pp. 226-260.
431 Gebrande H., 1986, CMP-Refraktionsseismik, in: Seismik auf neuen Wegen. Lothar Dresen,
432 Juergen Fertig, Horst Rueter, Wolfgang Budach, 191-205.
433 Geotomo. 2007. RES2DINV Ver. 3.56, Rapid 2-D resistivity and IP inversion using the least-
434 squares method. A, available at www.geoelectrical.com
435 Gibson B.S., Odegard M.E., Sutton G.H., 1979. Nonlinear least-squares inversion of traveltime
436 data for a linear velocity-depth relationship., Geophysics., Volume 44, 185-194.
437 Goldberg I., Gurevich B., 1998. A semi-empirical velocity–porosity–clay model for petrophysical
438 interpretation of P- and S-velocities. Geophysical Prospecting. 46, 271–285.
439 Gunn D.A., Chambers J.E., Uhlemann S., Wilkinson P.B., Meldrum P.I., Dijkstra T.A., Haslam E.,
440 Kirkham M., Wragg J., Holyoake S., Hughes P.N., Hen-Jones R., Glendinning S. 2015,
441 Moisture monitoring in clay embankments using electrical resistivity tomography.
442 Construction and Building Materials. 92, 82-94.
443 Haile T., Atsbaha S., 2014. Electrical resistivity tomography, VES and magnetic surveys for dam
444 site characterization, Wukro, Northern Ethiopia. Journal of African Earth Sciences., 97,
445 67-77.
446 Han D., Nur A., Morgan D., 1986. Effects of porosity and clay content on wave velocity of sand
447 stones. Geophysics. 51, 2093-2107.
448 Hickey C., Ekimov A., Hanson G., Sabatier J., 2010. "Time-Lapse Seismic Measurements on a
449 Small Earthen Embankment During an Internal Erosion Experiment." In SAGEEP 2009
450 Proceedings. Keystone, Colorado

451 ICOLD, 1995. Dam failures statistical analysis. The International Commission on Large Dams.
452 Bulletin 99, Paris.
453 Ikard S.J., Rittgers J., Revil A., Mooney M.A., 2015. Geophysical Investigation of seepage Beneath
454 an earthen dam. Groundwater. 53(2), 238-250.
455 Johansson S., Dahlin T., 1996. Seepage monitoring in an earth embankment dam by repeated
456 resistivity measurements. European J. Environ. Eng. journal of environmental and
457 engineering Geophysics, vol. 1(3): no, 3, pp. 229-247.
458 Kim J.H., Yi M.J., Song Y., Seol S.J., Kim K.S., 2007. "Application of geophysical methods to the
459 safety analysis of an earth dam. J. Environ. Eng. Geophysics. 12, 221-235.
460 Lee J.Y., Choi Y.K., Kim H.S.; Yun S.T., 2005. Hydrologic characteristics of a large rockfill dam:
461 Implications for water leakage. Engineering Geology, 80(1), 43-59.
462 Loperte, A., Soldovieri, F., Palombo, A., Santini, F., LLapenna, V., 2016. An integrated geophysical
463 approach for water infiltration detection and characterization at Monte Cotugno rock-
464 fill dam (southern Italy). Engineering Geology. 211, 162-170.
465 Loperte A., Soldovieri F., Lapenna V., 2015. Monte cotugno Cotugno dam monitoring by the
466 electrical resistivity tomography. IEEE J. Select. Top. Appl. Earth Obs. Remote Sensing.
467 8(11), 1-6.
468 Maslakowski M., Kowalczyk S., Mieszkowski R., Józefiak K., 2014. Using electrical resistivity
469 tomography (ERT) as a tool in geotechnical investigation of the substrate of a highway.
470 Stud. Quat. 31(2), 83–89.
471 McNeill J.D., 1980. Electromagnetic terrain conductivity measurement at low induction numbers
472 Geonics Limited, Technical Note TN-6, Canada, Mississauga, Ont.
473 McNeill J.D., 1990. Use of electromagnetic methods for groundwater studies, in: S.H. Ward, S.H.
474 ed., Geotechnical and Environmental Geophysics , Vol. I. Review & and Tutorial, Society
475 of Exploration Geophysicists, Oklahoma, USA, 191–218
476 Osazuwa I.B., Chii C.E., 2009. A two-dimensional electrical resistivity imaging of an earth dam,
477 Zaria. Nigeria Journal of Environmental Hydrology., vol. 17 (28) 1–8.
478 Rohdewald S., Burton B., Sheehan J., Doll W., 2010. Processing of seismic refraction tomography
479 data, SAGEEP short course notes, Keystone, Colorado.
480 Pavlovic V.D., Velickovic Z.S., 1998. Measurement of the seismic waves propagation velocity in
481 the real medium. Facta Universitatis: Phys. Chem. Technol. 1, 63–73.
482 Panthulu T.V., Krishnaiah C., Shirke J.M., 2001. Detection of seepage paths in earth dams using
483 self- potential and electrical resistivity methods. Engineering Geology. 59, 281-295.
484 Pérez-Flores M., Antonio-Carpio R., Gómez-Treviño E., Ferguson I.J., Méndez-Delgado S., 2011.
485 Imaging of 3D electromagnetic data at low-induction numbers. Geophysics. 77, 47–57.
486 Pislaru-Danescu L., Morega A. M., Morega M., Stoica V., 2013. New concept of measurement
487 apparatus for the in situ electrical resistivity of concrete structures, in Proc. 8th Int.
488 Symp. Adv. Topics Elect. Eng. (ATEE), pp. 1–6.
489 Seokhoon Oh., 2012. Electrical resistivity response due to variation in embankment shape and
490 reservoir levels. Environmental Earth Sciences. 65(:3), 571-579.
491 Sjödahl P., Dahlin T., Johansson S., Loke M.H., 2008. Resistivity monitoring for leakage and
492 internal erosion detection at Hällby embankment dam, Journal of Applied Geophysics.
493 65(3-4), 155-164.
494 Sudha K., Israil M., Mittal S., Rai J., 2009. Soil characterization using electrical resistivity
495 tomography and geotechnical investigations. J. Appl. Geophys. 67, 74–9.
496 Uromeihy A., Barzegari G., 2007. Evaluation and treatment of seepage problems at Chapar-Abad
497 Dam, Iran. Engineering Geology, 91(2), 219-228.

FIGURE CAPTIONS

Figure 1. a) Geological map of the study area (a modified version of www.igcc.cat) showing the different rock formations around the water reservoir. b) Digital elevation model of the study area. c) Geological cross-section parallel to the embankment.

Figure 2.a Sant Llorenç reservoir with the position of geophysical surveys on the embankment and the location of the land subsidence. 2.b Cross-section in the earth dam body. 2.c Example of sinkholes detected in the reservoir bed when it was emptied for maintenance in 1988.

Figure 3. Examples of refraction seismic shots recorded during the surveys. a) close to the concrete dam where the noise was high due to the hydroelectric plant (at the beginning of the dam), b) far from the hydroelectric plant (at 200 m from the beginning dam). The differences of noise in the signal are evident.

Figure 4. Inverted pseudo-sections of 8 ERT profiles with 2 m spacing between electrodes carried out in 2012 over the earthen embankment. ULRL: Upper Low Resistivity Layer, IHRL: Intermediate High Resistivity Layer and DLRL: Deeper Low Resistivity Layer.

Figure 5. Inverted pseudo-section of the concatenated ERT profile with 2 m spacing between electrodes along the earthen embankment carried out in 2003 and repeated in 2012.

Figure 6. Inverted model of the concatenated ERT profiles for the entire earthen embankment carried out in 2012 with 5 m spacing between electrodes.

Figure 7. Apparent EM conductivity measured along the earthen embankment with the Horizontal dipole (HD) and Vertical Dipole (VD).

Figure 8. a) Example of computed and observed traveltimes of the P. b) Wavepath coverage plot of line 3 after 10 WET (wavepath eikonal traveltime) wavepath coverage. The colour scale indicates the number of wavepaths through each velocity cell.

Figure 9. Inverted seismic refraction tomography pseudo-sections start off the distance 200 m of the levee because before this distance the noise produced by the hydropower plant was high.

Figure 10. Areas of concrete injections along the levee and the relative movement of the levee for different years.

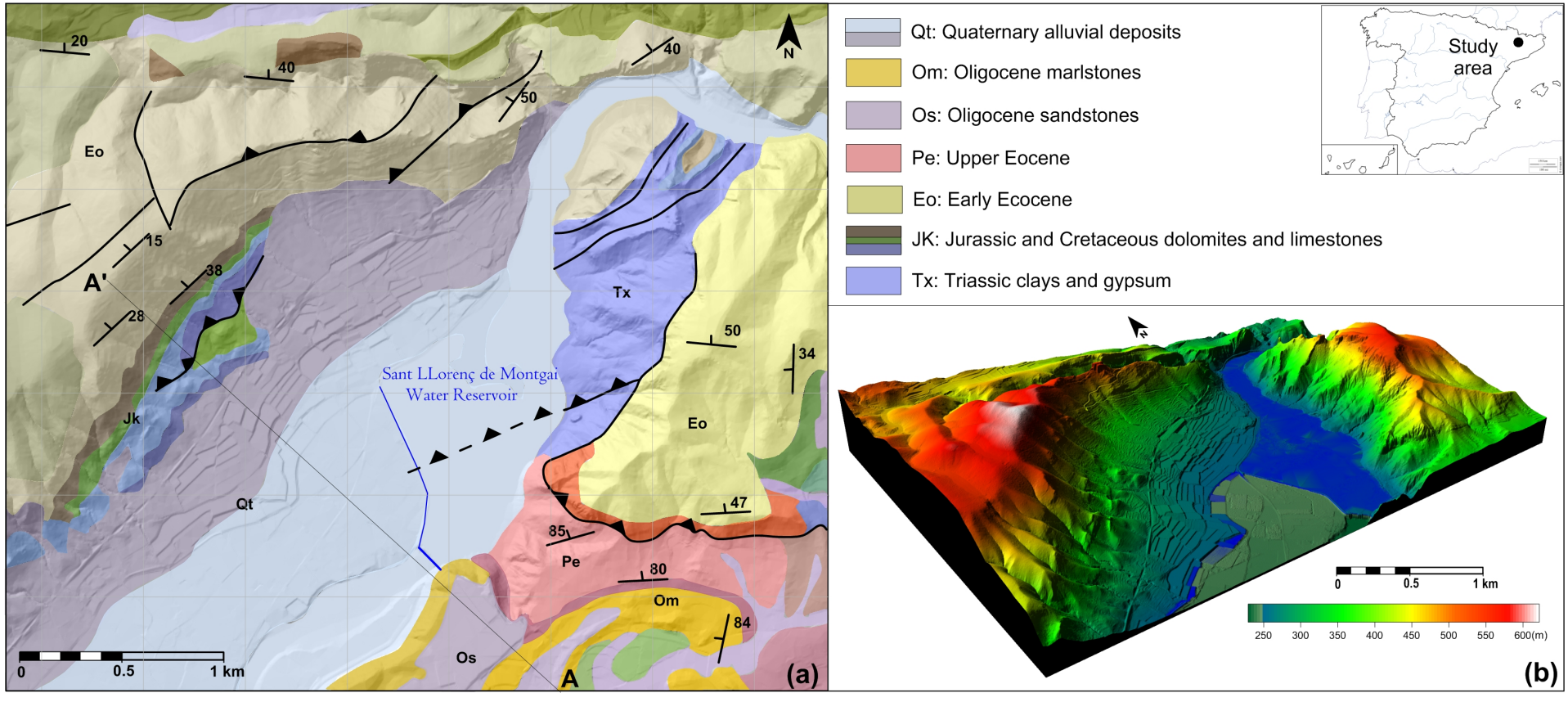
Qt: Quaternary alluvial deposits
Om: Oligocene marlstones
Os: Oligocene sandstones
Pe: Upper Eocene
Eo: Early Ecocene
JK: Jurassic and Cretaceous dolomites and limestones
Tx: Triassic clays and gypsum
Study area
N
Sant LLorenç de Montgai Water Reservoir
A
A'
Eo
Jk
Qt
Tx
Pe
Om
Os
20
40
40
50
15
38
28
50
34
47
85
80
84
0
0.5
1 km
(a)
250
300
350
400
450
500
550
600(m)
(b)

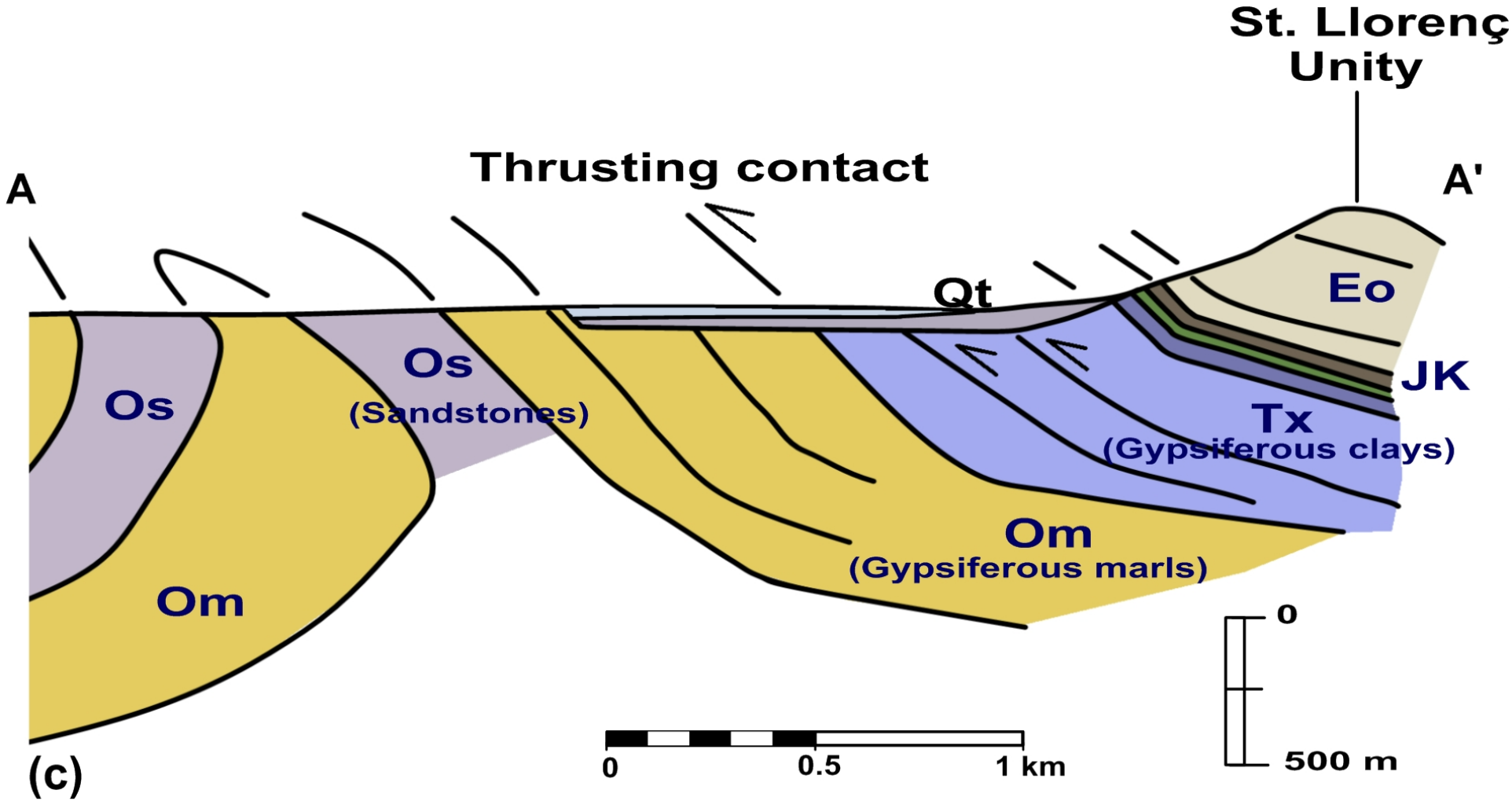
St. Llorenç
Unity
Thrusting contact
A
A'
Qt
Eo
JK
Tx
(Gypsiferous clays)
Os
(Sandstones)
Os
Om
(Gypsiferous marls)
Om
0
500 m
0
0.5
1 km
(c)

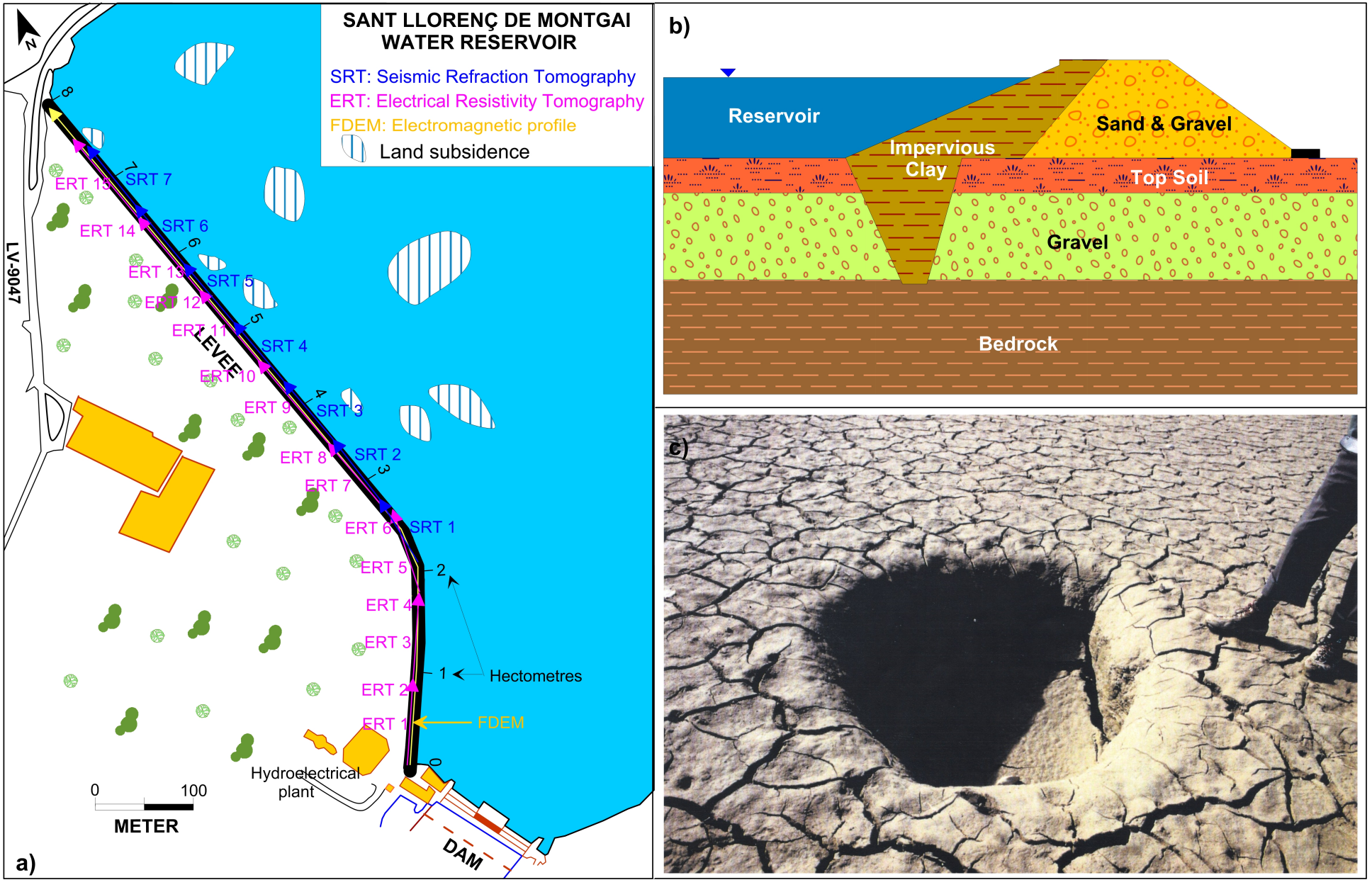
SANT LLORENÇ DE MONTGAI
WATER RESERVOIR
SRT: Seismic Refraction Tomography
ERT: Electrical Resistivity Tomography
FDEM: Electromagnetic profile
Land subsidence
N
LV-9047
LEVEE
ERT 15
ERT 14
ERT 13
ERT 12
ERT 11
ERT 10
ERT 9
ERT 8
ERT 7
ERT 6
ERT 5
ERT 4
ERT 3
ERT 2
ERT 1
SRT 7
SRT 6
SRT 5
SRT 4
SRT 3
SRT 2
SRT 1
8
7
6
5
4
3
2
1
0
Hectometres
FDEM
Hydroelectrical plant
DAM
0
100
METER
a)
b)
Reservoir
Impervious Clay
Sand & Gravel
Top Soil
Gravel
Bedrock
c)

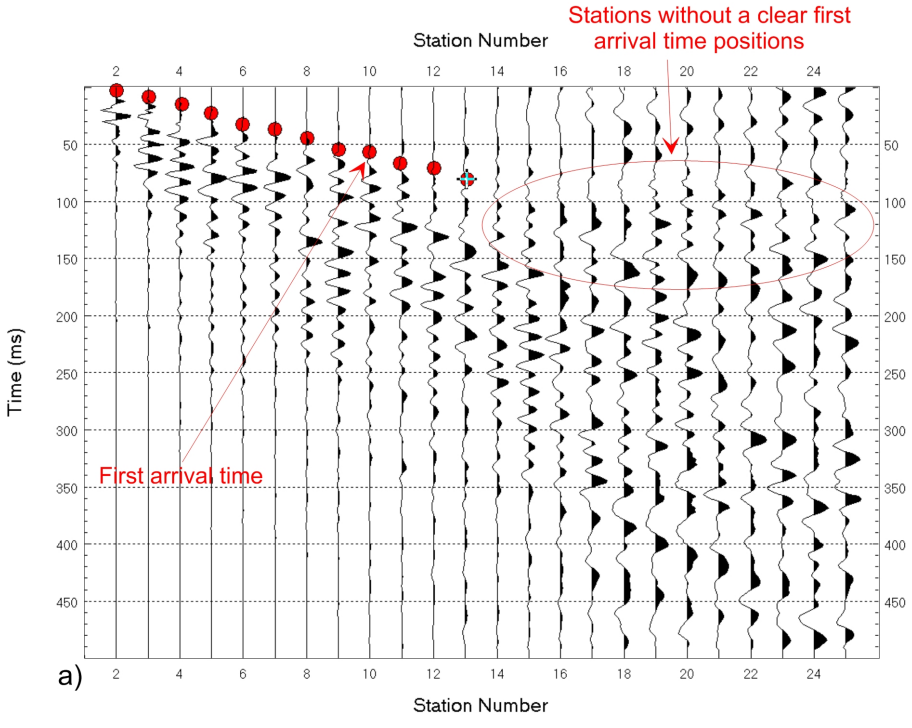
Stations without a clear first arrival time positions
Station Number
Time (ms)
First arrival time
a)
Station Number

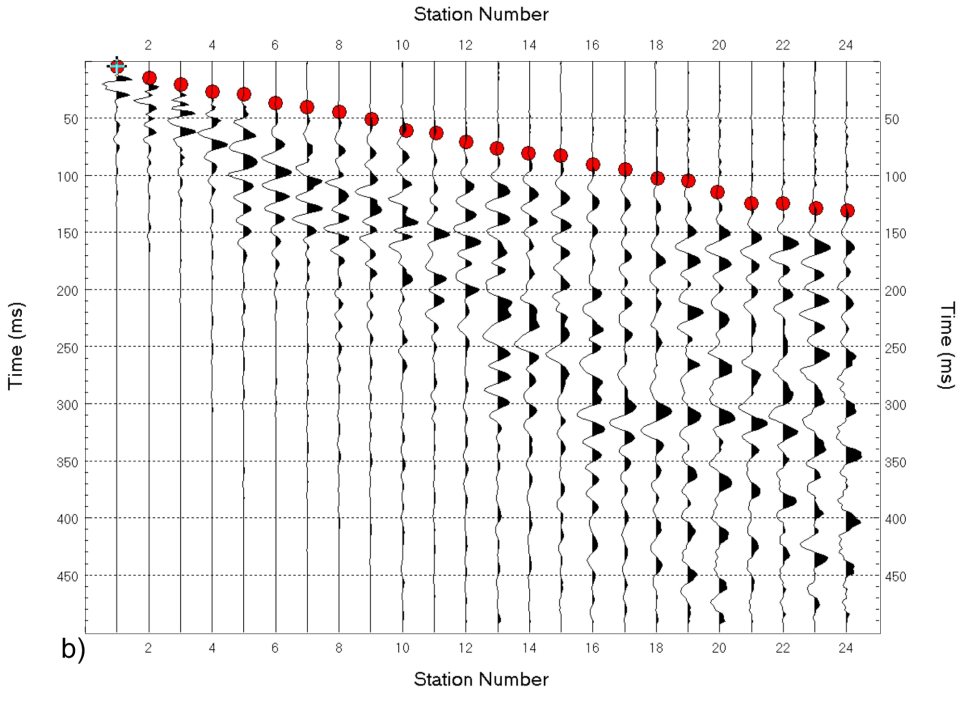
Station Number
Time (ms)
b)
Station Number

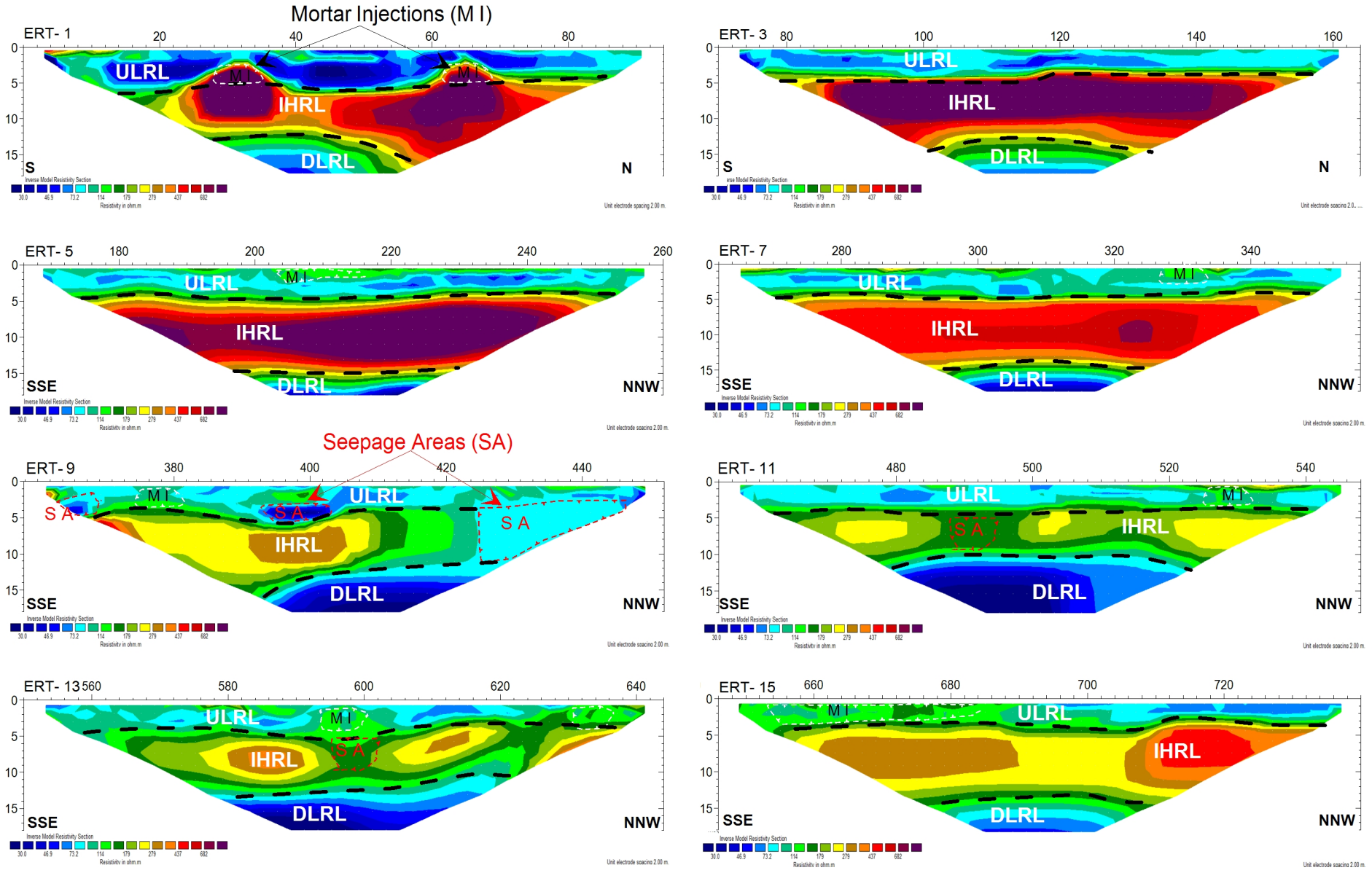
Mortar Injections (M I)
ERT- 1
20
40
60
80
ULRL
M I
M I
IHRL
DLRL
S
N
ERT- 3
80
100
120
140
160
ULRL
IHRL
DLRL
S
N
ERT- 5
180
200
220
240
260
ULRL
M I
IHRL
DLRL
SSE
NNW
ERT- 7
280
300
320
340
ULRL
M I
IHRL
DLRL
SSE
NNW
Seepage Areas (SA)
ERT- 9
380
400
420
440
M I
S A
S A
ULRL
S A
IHRL
DLRL
SSE
NNW
ERT- 11
480
500
520
540
ULRL
M I
S A
IHRL
DLRL
SSE
NNW
ERT- 13
560
580
600
620
640
ULRL
M I
IHRL
S A
DLRL
SSE
NNW
ERT- 15
660
680
700
720
M I
ULRL
IHRL
DLRL
SSE
NNW
0
5
10
15
Inverse Model Resistivity Section
30.0
46.9
73.2
114
179
279
437
682
Resistivity in ohm.m
Unit electrode spacing 2.00 m.

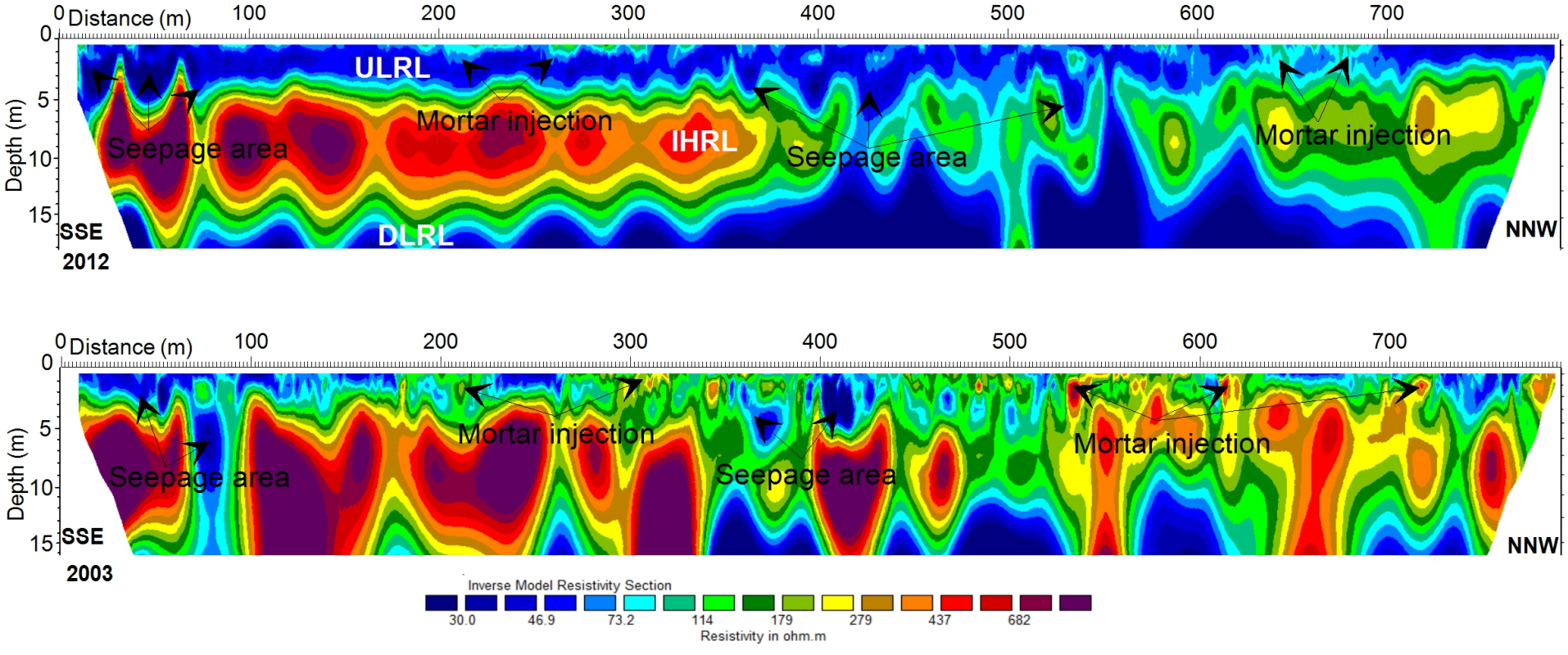
0
Distance (m)
100
200
300
400
500
600
700
Depth (m)
0
5
10
15
ULRL
Mortar injection
IHRL
Seepage area
Seepage area
Mortar injection
DLRL
SSE
NNW
2012
0
Distance (m)
100
200
300
400
500
600
700
Depth (m)
0
5
10
15
Mortar injection
Seepage area
Seepage area
Mortar injection
SSE
NNW
2003
Inverse Model Resistivity Section
30.0
46.9
73.2
114
179
279
437
682
Resistivity in ohm.m

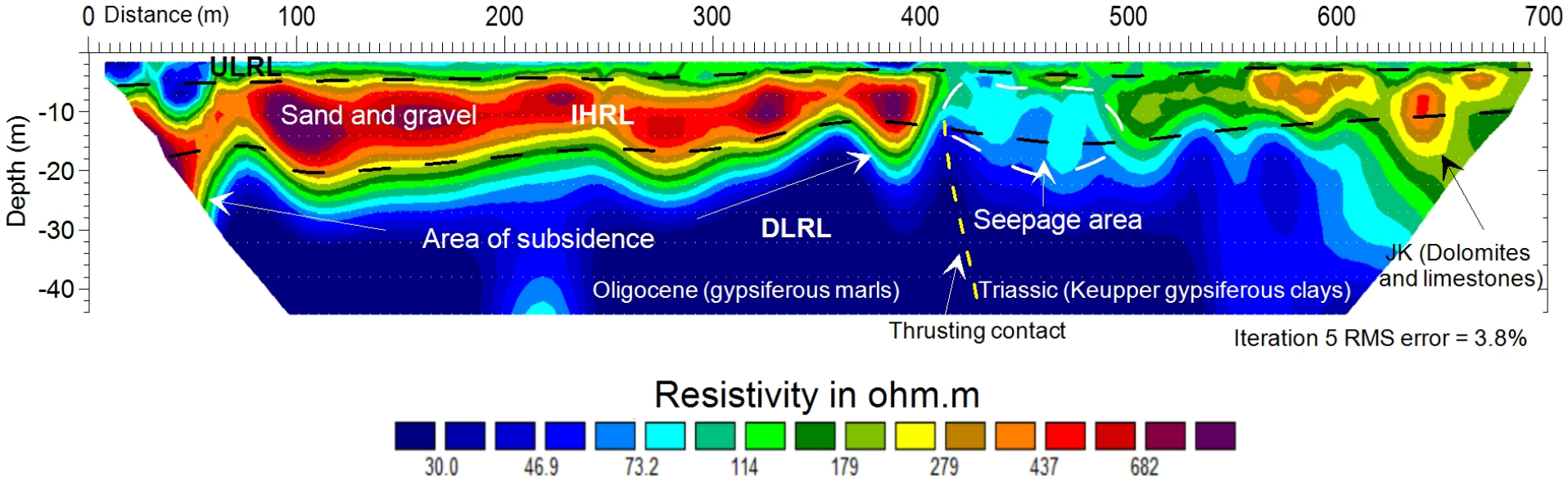
0 Distance (m)
100
200
300
400
500
600
700
Depth (m)
-10
-20
-30
-40
ULRL
Sand and gravel
IHRL
Area of subsidence
DLRL
Seepage area
JK (Dolomites and limestones)
Oligocene (gypsiferous marls)
Triassic (Keupper gypsiferous clays)
Thrusting contact
Iteration 5 RMS error = 3.8%

Resistivity in ohm.m
30.0
46.9
73.2
114
179
279
437
682

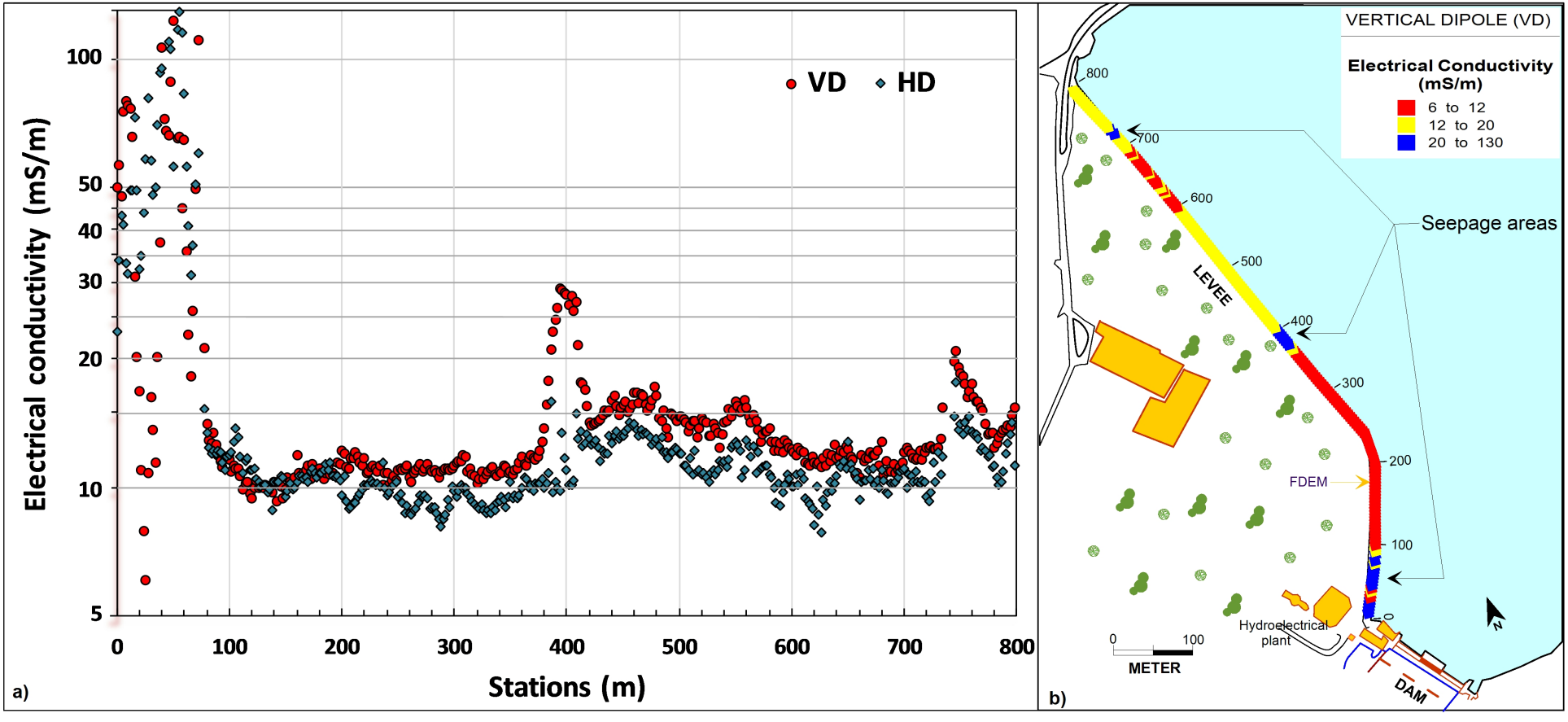
Electrical conductivity (mS/m)
100
50
40
30
20
10
5
VD
HD
0
100
200
300
400
500
600
700
800
Stations (m)
a)
VERTICAL DIPOLE (VD)
Electrical Conductivity (mS/m)
6 to 12
12 to 20
20 to 130
800
700
600
500
400
300
200
100
0
LEVEE
Seepage areas
FDEM
Hydroelectrical plant
DAM
0
100
METER
N
b)

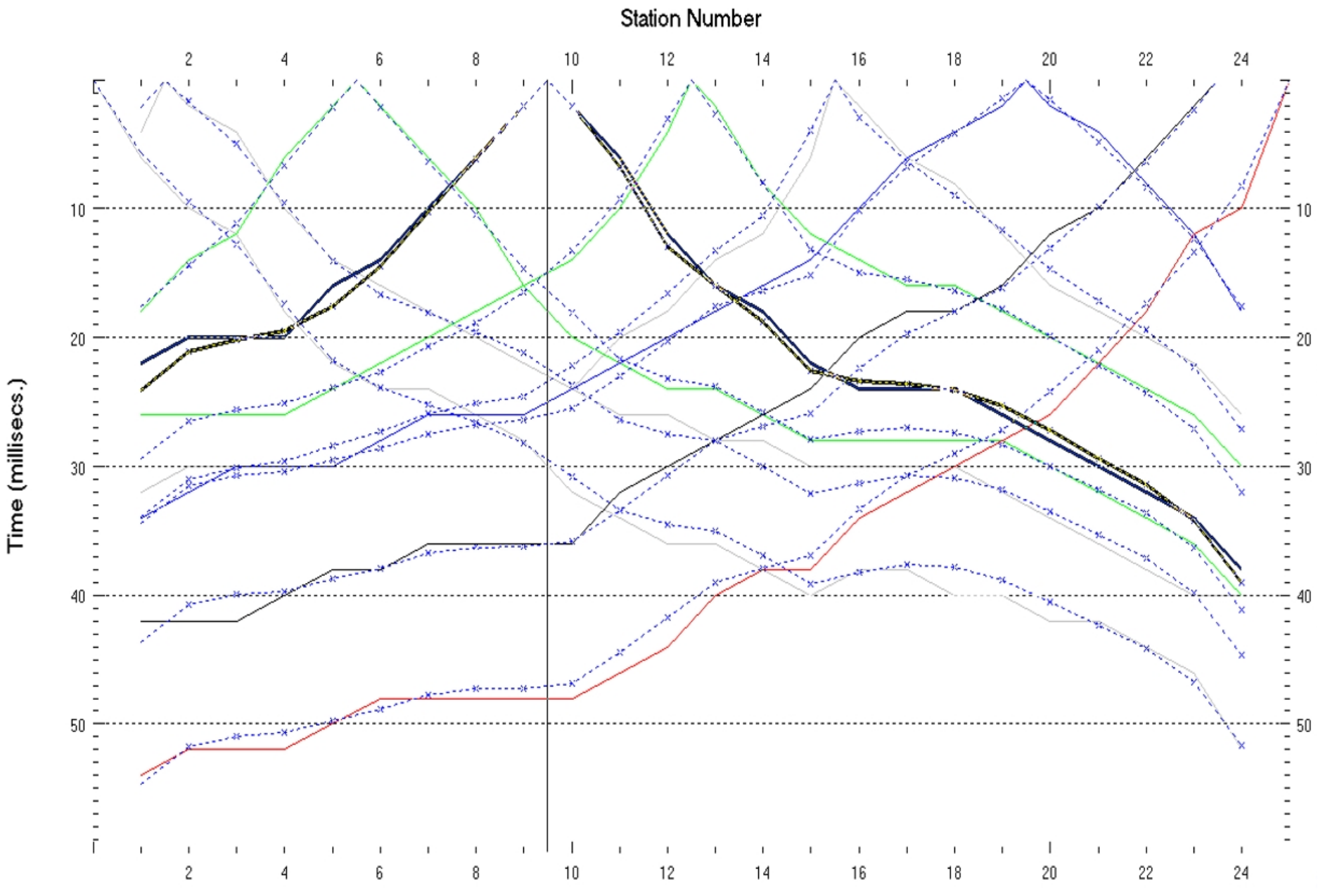
Station Number
2
4
6
8
10
12
14
16
18
20
22
24
Time (millisecs.)
10
20
30
40
50

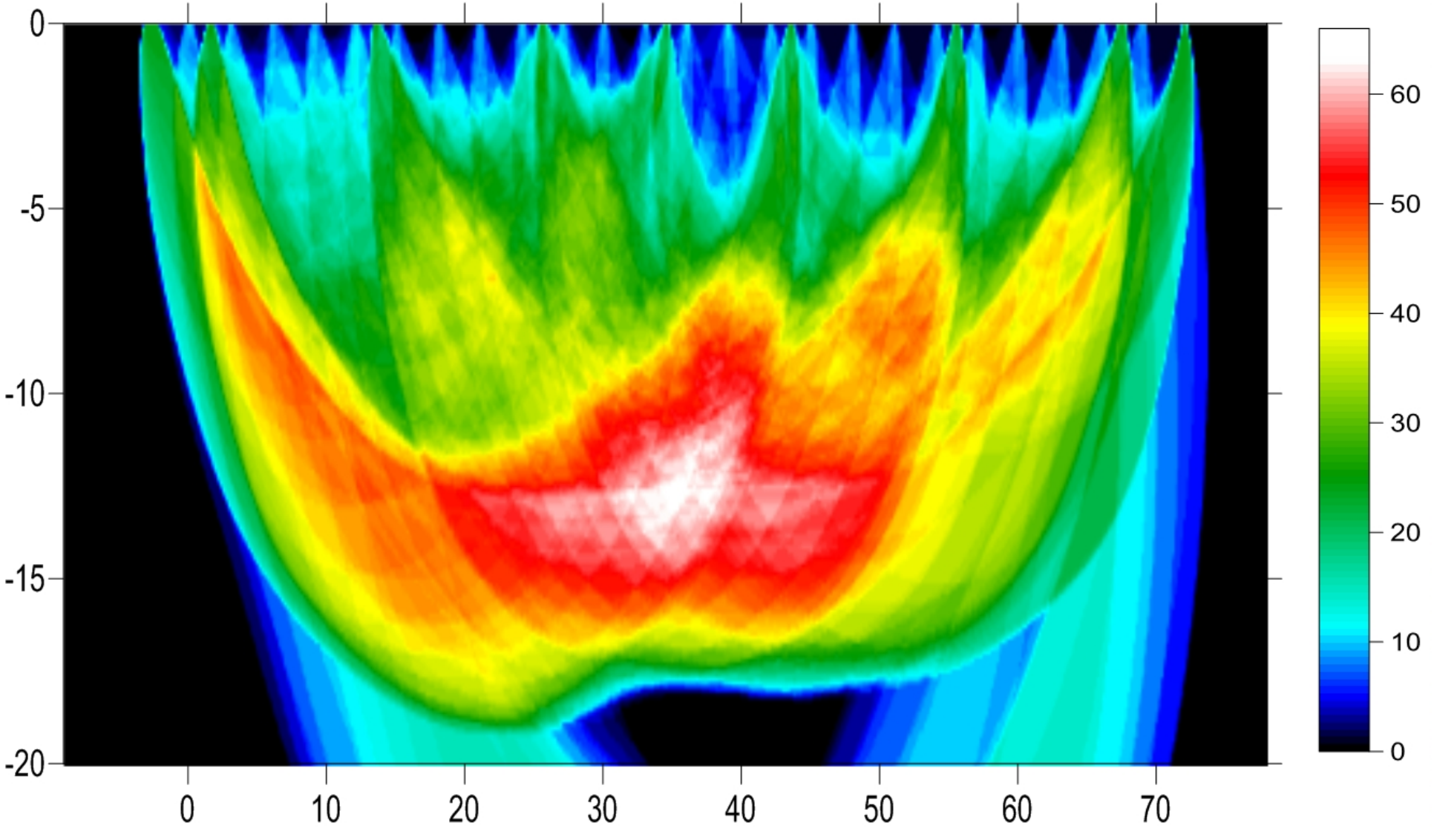
L3, 10 WET iterations, RMS error 3.2 %, 1D-Gradient smooth initial model, Version 3.17
0
-5
-10
-15
-20
0
10
20
30
40
50
60
70
60
50
40
30
20
10
0

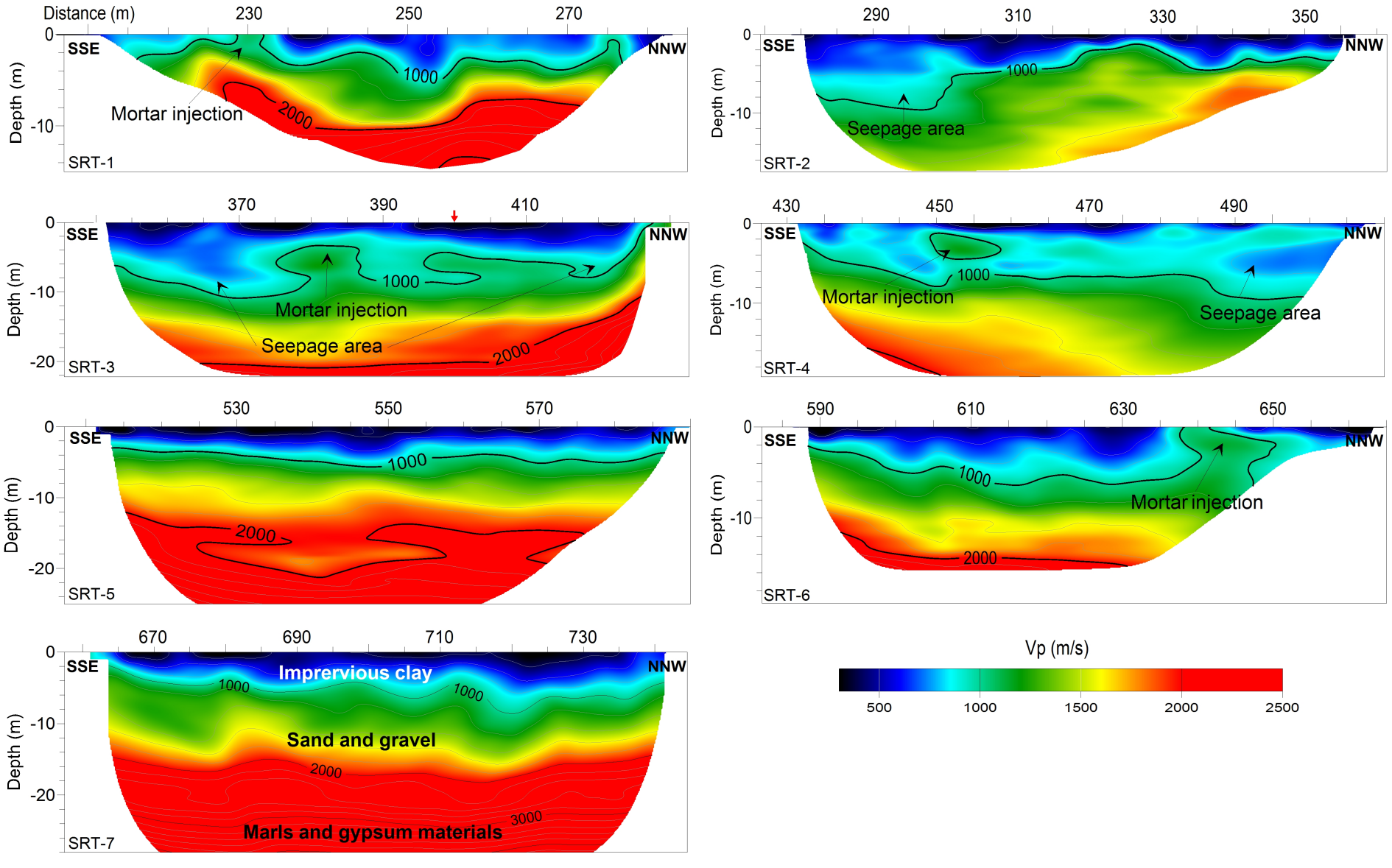
Distance (m)
230
250
270
SSE
NNW
Depth (m)
0
-10
1000
2000
Mortar injection
SRT-1
290
310
330
350
Seepage area
SRT-2
370
390
410
-20
Mortar injection
Seepage area
SRT-3
430
450
470
490
Mortar injection
Seepage area
SRT-4
530
550
570
SRT-5
590
610
630
650
Mortar injection
SRT-6
670
690
710
730
Imprervious clay
Sand and gravel
3000
Marls and gypsum materials
SRT-7
Vp (m/s)
500
1000
1500
2000
2500

Distance	0	100	200	300	400	500	600	700
Years								
2009	■	■	■	■				
2007				■	■	■		
2000			■	■				
1998		■	■		■			
1993							■	■
1991	■	■	■	■			■